Eur. Phys. J. E **27**, 37–46 (2008)
DOI 10.1140/epje/i2008-10349-8

THE EUROPEAN PHYSICAL JOURNAL E

Frictional properties of confined polymers

I.M. Sivebaek[1,2,3], V.N. Samoilov[1,4], and B.N.J. Persson[1,a]

[1] IFF, FZ-Jülich, 52425 Jülich, Germany
[2] Novo Nordisk A/S, Research and Development, DK-3400 Hillerod, Denmark
[3] Department of Mechanical Engineering, Technical University of Denmark, DK-2800 Lyngby, Denmark
[4] Physics Faculty, Moscow State University, 117234 Moscow, Russia

Received 25 February 2008 and Received in final form 11 April 2008
Published online: 24 July 2008 –

Abstract. We present molecular dynamics friction calculations for confined hydrocarbon solids with molecular lengths from 20 to 1400 carbon atoms. Two cases are considered: a) polymer sliding against a hard substrate, and b) polymer sliding on polymer. In the first setup the shear stresses are relatively independent of molecular length. For polymer sliding on polymer the friction is significantly larger, and dependent on the molecular chain length. In both cases, the shear stresses are proportional to the squeezing pressure and finite at zero load, indicating an adhesional contribution to the friction force. The friction decreases when the sliding distance is of the order of the molecular length indicating a strong influence of molecular alignment during run-in. The results of our calculations show good correlation with experimental work.

PACS. 31.15.Xv Molecular dynamics and other numerical methods – 62.20.Qp Friction, tribology, and hardness – 68.35.Af Atomic scale friction

1 Introduction

Tribology is the science and technology of surfaces in contact in relative sliding motion. The subject is of huge practical and theoretical importance as lubrication, friction and wear are key properties in almost all applications with moving parts [1, 2].

In medical devices designed for injecting medicine through the human skin polymer materials are extensively used. In some devices polymers are used against hard substrates but predominantly polymer against polymer contacts are seen. Most of the devices are driven manually by the hand of the patient so low dosage force is a prerequisite in device conception. At Novo Nordisk several millions of such devices are produced yearly so the price of the used polymeric material is also of significant importance. The challenge is to control and lower the friction between these low-cost materials without external lubrication as this is banned in a high volume production.

Very little information is available in the literature concerning friction between polymers whereas the frictional properties between polymer and metal surfaces have been extensively investigated [3]. One of us [4] has developed an experimental method capable of establishing the tribological properties of polymeric materials. The method uses two injection molded circular polymeric specimens which are slid against each other (rotational motion) at varying sliding velocities, normal pressures, relative humidities and temperatures [4]. The results can be used when designing new medical devices and the investigations have led to the discovery of new tribologically favorable polymeric compounds never envisaged before.

In the experiments it has been observed that the friction between two identical polymeric materials is always very high and erratic whereas replacement of one of the materials with a different one typically divides the friction by at least three (see Fig. 1). Note also that the nominal shear stress is (approximately) proportional to the applied pressure. This result is expected since the sliding systems are most likely of the multi-asperity contact type, where one expects a linear dependence of the real area of contact on the applied pressure as long as the area of real contact is small compared to the nominal contact area. Since the typical shear stress when polymer slides on polymer (complete contact) is of the order of $\sim$ 20–40 MPa at low normal pressures (see below), the area of real contact A in the experiment reported on in Figure 1 is likely to be of the order of a few % of the nominal contact area A_0. The same fractional contact area is expected from the penetration hardness σ_Y of the polymers (which is $\sigma_Y \approx 0.1$–0.3 GPa) and the applied nominal pressures p in Figure 1 ($A/A_0 \approx p/\sigma_Y \approx 0.01$).

Experimental data in the literature indicate that both the friction between a polymer and a metal and between polymers is a consequence of a shearing of polymeric material [5]. In general a polymeric film is sheared also in the

[a] e-mail: B.Persson@fz-juelich.de

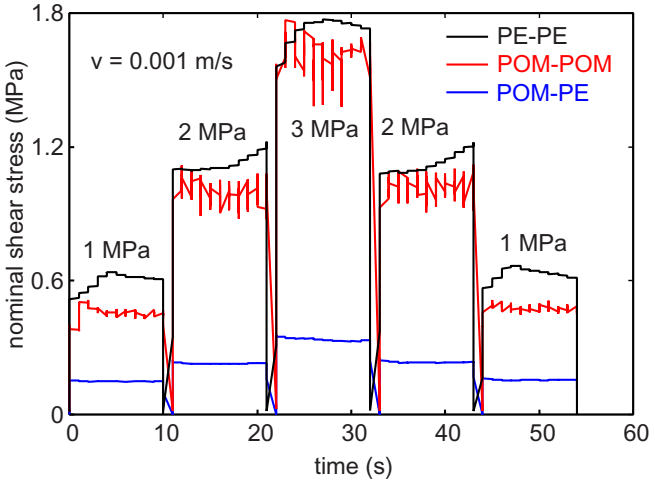

Fig. 1. The nominal frictional stress for acetal sliding on acetal (polyoxymethylene, POM), for polyethylene (PE) sliding on polyethylene and for polyethylene sliding on acetal. Experiment at room temperature with sliding velocity $v = 0.001\,\mathrm{m/s}$ and the nominal applied pressure $p = 1$, 2 and 3 MPa.

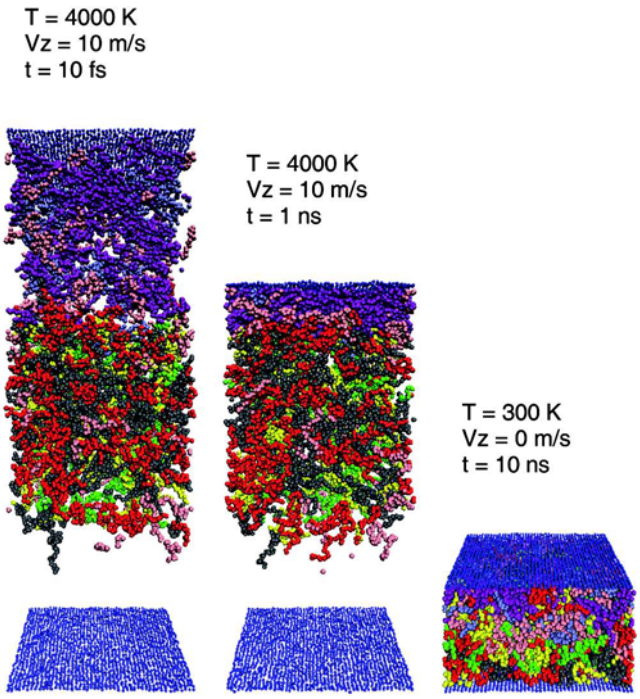

Fig. 2. Snapshot pictures of the polymer-solid wall system during the preparation phase. The polymer system is initially in a hot ($T \approx 4000\,\mathrm{K}$) gas-like state, and slowly cools down by colliding with the solid walls. When the temperature has fallen enough the molecules condense on the solid walls. The preparation phase for $C_{60}H_{122}$ "metal"-polymer system is shown.

polymer-metal case as a polymeric film is transferred to the hard surface resulting in friction originating from the shear of this film [3, 5, 6].

Shearing of polymers is characterized by an initial aligning of the molecules. After this alignment of the molecules (run-in phase) the shear stress decreases significantly [3, 5–9]. Increasing the normal pressure in a polymeric contact also increases the shear stress. At low normal pressures the main contribution to the shear stress comes from adhesion which is constant. At higher normal pressures the shear stress becomes proportional to the applied pressure [5, 8, 10–12].

In the following we present Molecular Dynamics (MD) calculations for confined polyethylene with chain lengths from 20 to 1400 carbon atoms. MD calculations for confined polymer films have been presented in several earlier papers [13] but we use larger systems, a wider distribution of chain lengths, and a more accurate way of removing the frictional heat from the sliding system, than in earlier publications. We also present for the first time a detailed study of the modifications of the polymer film during run-in, which requires exceptionally long (for MD) simulation time periods. We note that in these theoretical calculations most parameters, such as contact area, are easier to control than in experiments. Thus MD calculations present an important supplement to experiments in order to understand polymer friction.

In Section 2 we describe the model used in the present study. In Section 3 we study run-in. We show that, in particular for the longest hydrocarbon chains, very long run-in distances (in the context of MD simulations) are necessary before reaching a steady state. In Section 4 we study the pressure dependence of the frictional shear stress. We find a linear dependence of the frictional shear stress on the squeezing pressure, as also observed in some earlier studies, both for the polymer-polymer and polymer-substrate sliding interfaces. However, in the latter case both the shear stress and the rate at which it increases with increasing pressure is much smaller, and we explain this with a simple model. Section 5 contains the summary and conclusions.

2 The model

In this paper we present computer simulations and analytical argument about the frictional behavior of linear hydrocarbons under applied pressure. Our model is similar to those described in references [14–16], but we review its main features here. We consider a block and a substrate with atomically flat surfaces separated by a polymer slab. Two cases are considered: a) polymer sliding against a hard substrate which we will denote as "metal" for simplicity (the metal-polymer case), and b) polymer sliding on polymer (the polymer-polymer case).

The solid walls are treated as single layers of "atoms" bound to rigid flat surfaces by springs corresponding to the long-range elastic properties of 50 Å thick solid slabs. Periodic boundary conditions were used in x- and y-directions, similar to references [14–16].

The systems were prepared in the following way (see Fig. 2). We started with large distance between the substrate and the block surfaces (several hundred Å) and high temperatures (usually several thousand K) so that alkane molecules were in the gas-like phase. The temperature of

the solid walls was kept close to 300 K by coupling the substrate and the block atoms to a thermostat. Due to frequent collisions of the alkane molecules with the walls, the gas cooled down and condensed on the solid walls. The cooling down process was simulated together with decreasing the distance between the walls. After around 10 ns the system reached thermal equilibrium at the temperature 300 K. For the case of sliding of polymer on "metal", all molecules adsorbed on the block surface only due to different parameters of interaction of alkane molecules with the walls, whereas for the case of sliding of polymer on polymer about a half of the molecules adsorbed on the block surface and a half on the substrate surface. Then the polymer was put into contact with the substrate surface in the first case and two polymer slabs were put into contact in the second case and after equilibrium temperature (300 K) was achieved we started to move the block surface.

The molecular dynamics calculations have been performed by keeping the temperature of the solid walls fixed. This is a realistic treatment, and it implies that heat flows from the polymer to the confining walls. In the present calculations the temperature of the solid walls was equal to 300 K.

Linear alkanes C_nH_{2n+2} (with n ranging from 20 to 1400) were used as "lubricant" in the present calculations. The CH_2/CH_3 beads are treated in the united atom representation [17,18]. The Lennard-Jones potential was used to model the interaction between beads of different chains

$$U(r) = 4\epsilon_0 \left[\left(\frac{r_0}{r}\right)^{12} - \alpha \left(\frac{r_0}{r}\right)^{6} \right], \qquad (1)$$

and the same potential with modified parameters (ϵ_1, r_1) was used for the interaction of each bead with the substrate and block atoms. The parameters were $\epsilon_0 = 5.12$ meV for both the interior and end beads and $r_0 = 3.905$ Å and $\alpha = 1$ in all cases. For the interactions within the C_nH_{2n+2} molecules we used the standard OPLS model [17,18], including flexible bonds, bond bending and torsion interaction, which results in bulk properties in good agreement with experimental data.

For polymer sliding on polymer we need the polymer-metal bond to be so strong that no slip occurs at these interfaces. This is the case with $r_1 = 3.28$ Å, $\epsilon_1 = 40$ meV and $\alpha = 3$. We also did some simulations with $\alpha = 2$, but in this case some slip was observed at the polymer-metal interface.

For sliding of polymer on "metal" we used the same parameters as above for the polymer-block interaction. For the polymer-substrate interaction we used $\alpha = 1$ and $\epsilon_1 = 10$ meV.

The choice of higher values of ϵ_1 compared to ϵ_0 reflects the stronger (van der Waals) interaction between the beads and "metal" surfaces than between the bead units of different lubricant molecules (this stronger interaction results from the higher electron density in the metals). The lattice spacings of the block and of the substrate are $a = b = 2.6$ Å.

We used linear alkane molecules with the number of carbon atoms 20, 60, 100, 140 and 1400 as lubricant. The number of $C_{100}H_{202}$ molecules was equal to 200. The number of $C_{20}H_{42}$ molecules was equal to 1000. This gave from 6 to 8 monolayers of lubricant molecules between the solid surfaces. The (nominal) squeezing pressure p_0 was varied from 0 to 3 GPa.

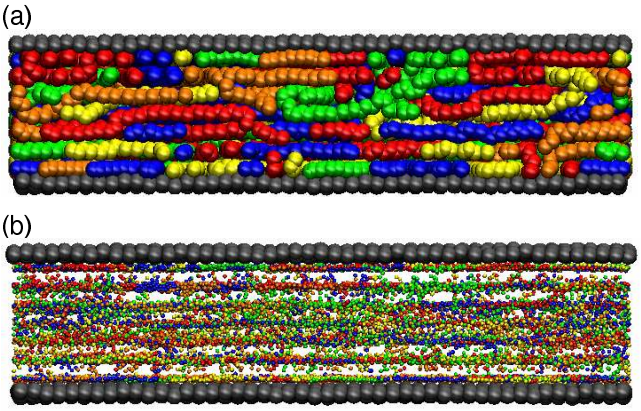

Fig. 3. (Colour on-line) Snapshot picture of the $C_{100}H_{202}$ polymer slab after run-in at the sliding velocity $v = 10$ m/s and background temperature $T = 300$ K. (a) The molecules are (arbitrarily) colored in order to better observe the shear alignment of the chains. (b) The same as in (a) but with atoms presented as points in order to observe layering in the system. Seven monolayers of molecules are clearly seen.

As an illustration, in Figure 3 we show the contact between a flat elastic block (top) and a flat elastic substrate (bottom). The polymer slab (~ 30 Å thick) is between them. Only the interfacial block and substrate atoms and polymer atoms are shown.

3 Run-in

In general, we find that the run-in distance increases as the length of the alkane molecules increases. We did some studies with different sliding velocity which indicate that not only the sliding distance but also the sliding velocity matter for the degree of run-in. This is in accordance with experimental data [19]. During the run-in time period rearrangement in the polymer film takes place. This rearrangement is larger for the sliding of polymer on polymer than for the sliding of polymer on metal due to much higher corrugation felt by polymer molecules sliding in contact with the same kind of polymer molecules.

The run-in distance is especially long for the $C_{1400}H_{2802}$ polymer-polymer interface, and results in a strong decrease in the shear stress (see Fig. 4). The maximal value of the shear stress for $C_{1400}H_{2802}$ during run-in is ~ 8 times higher than the shear stress value after run-in. In the initial state (before sliding) each of the $C_{1400}H_{2802}$ molecules binds to both solids walls, and the large initial shear stress in Figure 4 corresponds to stretching the molecules between the two surfaces (see Fig. 5 for the behavior of one polymer molecule in the film). The polymer-solid wall bond is very strong (in order to avoid wall slip after run-in), and the polymers are stretched to a length of ~ 2000 Å (or more) before the bond breaks to

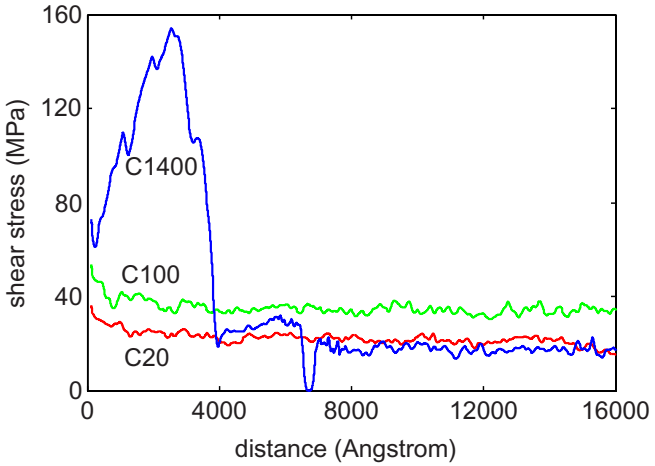

Fig. 4. The shear stress for $C_{20}H_{42}$, $C_{100}H_{202}$ and $C_{1400}H_{2802}$ polymer-polymer during run-in at the sliding velocity $v = 100\,\mathrm{m/s}$ and the applied pressure $p = 10\,\mathrm{MPa}$. The strong variations in the shear stress reflect changes in the structure of the polymer films during run-in.

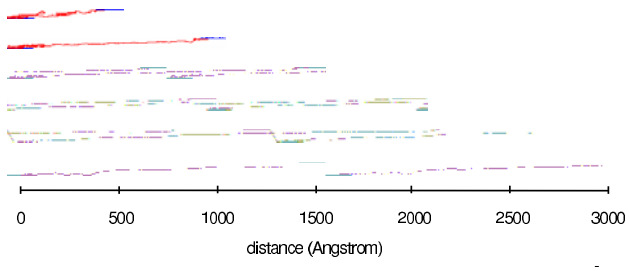

Fig. 5. Stretching of a $C_{1400}H_{2802}$ polymer molecule in the polymer film during sliding. The bond to the bottom surface of the block breaks after the sliding distance $\sim 2000\,\text{Å}$.

one of the walls. In reality, chain scission may occur under these circumstances, but this is not allowed in our model. The sharp drop in the shear stress at the sliding distance $\sim 3000\,\text{Å}$ is associated with breaking polymer–solid-wall bonds in such a way that for larger sliding distances each polymer molecule is bound to only one wall (and roughly half of them to each wall). A rearrangement of the polymer molecules takes place during run-in, so that after run-in the molecules tend to align in the direction of motion of the block, which results in lower shear stress. Thus the shear stress for $C_{1400}H_{2802}$ becomes lower than for $C_{20}H_{42}$.

The results in Figure 4 are for the sliding velocity $v = 100\,\mathrm{m/s}$, but even at this relatively high sliding velocity the frictional energy dissipation in the polymer film gives rise to negligible temperature increase. The reason for this is that the polymer film is very thin, and that the wall atoms are coupled to a thermostat (at temperature $T = 300\,\mathrm{K}$) so that the excess (friction-induced) thermal energy is effectively removed from the system, leading to the negligible temperature increase.

In Figure 6 we show the changes in alignment of $C_{20}H_{42}$ and $C_{100}H_{202}$ molecules for polymer sliding on polymer at the velocity $v = 10\,\mathrm{m/s}$, and for the applied pressure $p = 10\,\mathrm{MPa}$. For $C_{100}H_{202}$ the molecules become

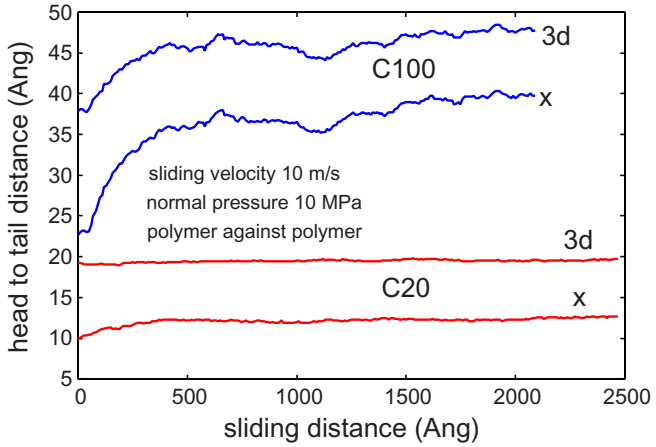

Fig. 6. Changes in alignment of $C_{20}H_{42}$ and $C_{100}H_{202}$ molecules for polymer-polymer during run-in at velocity $v = 10\,\mathrm{m/s}$ and for the applied pressure $p = 10\,\mathrm{MPa}$. For $C_{100}H_{202}$ the molecules become more elongated in the sliding x-direction and also their head to tail length increases, *i.e.* they become more straight.

more (almost twice) elongated in the sliding x-direction and also their head to tail length increases, *i.e.* they become more straight. Alignment of the molecules in the $C_{20}H_{42}$ polymer film is much smaller. Note, however, that the head to tail length of the $C_{100}H_{202}$ molecules is only ~ 2 times longer than that of $C_{20}H_{42}$ while the number of carbon atoms is 5 times more. The reason for this of course is that $C_{20}H_{42}$ is more "rod-like" than the longer chain $C_{100}H_{202}$. However, the persistence length for long alkanes is of the order of $\sim 0.5\,\mathrm{nm}$ [20] so one would expect that even $C_{20}H_{42}$ has, on the average, some curvature. (The natural length of the $C_{20}H_{42}$ is about $23.75\,\text{Å}$ which is slightly longer than the (average) head to tail distance $\approx 20\,\text{Å}$ in Fig. 6.) However, as we will show below, the $C_{20}H_{42}$ film consists, at least in part, of small three-dimensional (3D) crystalline regions (lamella), where the chains are straight and parallel.

In our previous calculations of sliding and squeezing with the linear alkanes we observed areas of one monolayer thick lubricant film in which the molecules were aligned almost parallel to each other (2D domains). This alignment was observed for one monolayer thick lubricant films, for instance, before expelling the last monolayer of lubricant molecules during squeezing. In the present calculations we observe 3D regions of $C_{20}H_{42}$ in which the molecules are aligned almost parallel to each other. In Figure 7 we show the views on the $C_{20}H_{42}$ metal-polymer system (the same as presented in Fig. 8) at two different angles. The 3D domains of ordered $C_{20}H_{42}$ molecules are clearly seen, with the molecular backbones parallel to each other and subtending an angle $\approx 70°$ to the lamellar plane, which is very similar to that of bulk $C_{20}H_{42}$ [21]. In this metal-polymer sliding system sliding occurs only at the interface between the first monolayer of polymer molecules and the substrate. During sliding the domains remain almost the same, their boundaries only slightly change, but stronger alignment of the domains at the sliding surface may occur

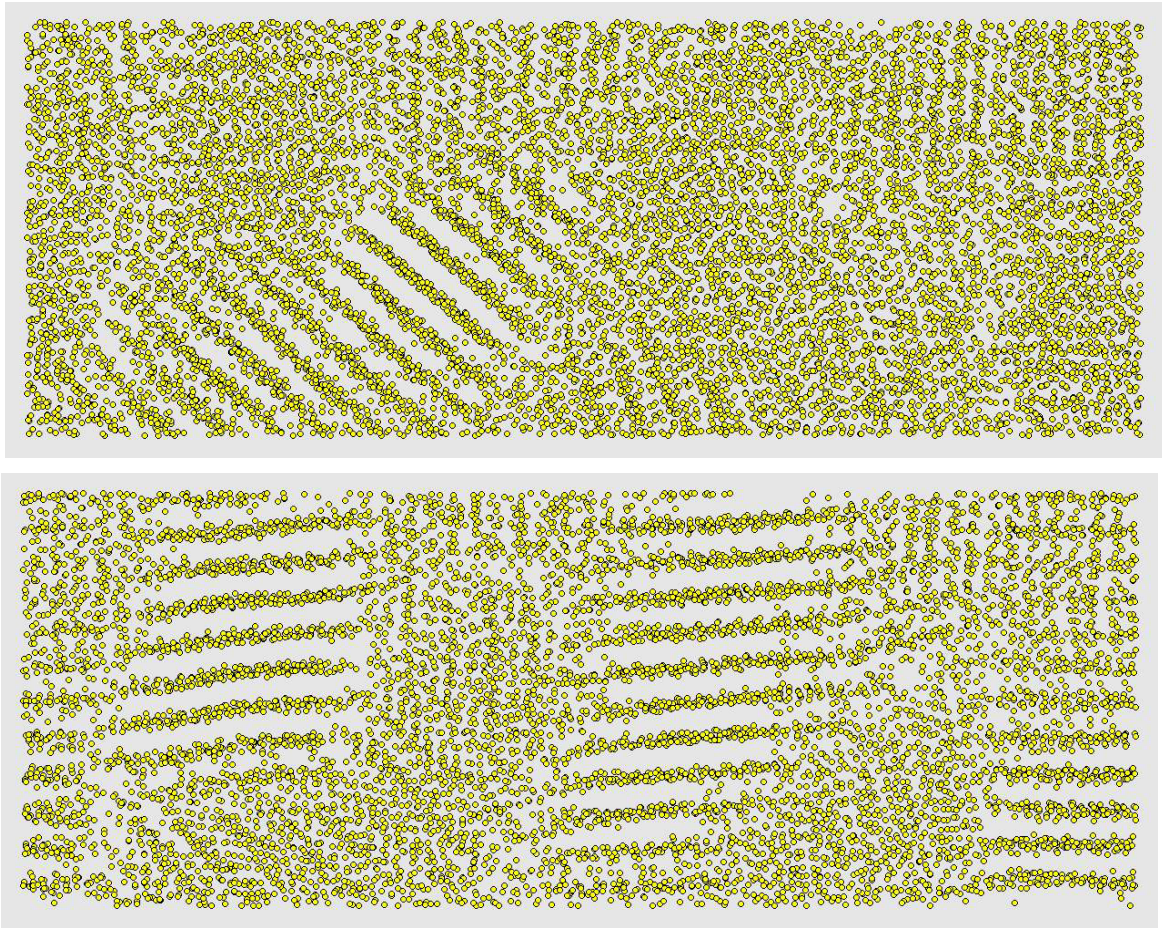

Fig. 7. The views on the $C_{20}H_{42}$ metal-polymer system (the same as presented in Fig. 8) at two different angles 45° (upper snapshot) and 30° (lower snapshot) from the z-direction (rotation in the yz-plane). The system includes 1000 $C_{20}H_{42}$ lubricant molecules. Applied pressure $p = 10\,\text{MPa}$; temperature $T = 300\,\text{K}$. The block is moving to the right with velocity $v = 10\,\text{m/s}$. The system is presented after sliding the distance 1400 Å. Only CH_2/CH_3 beads of lubricant molecules are shown. The 3D domains of aligned $C_{20}H_{42}$ molecules are clearly seen.

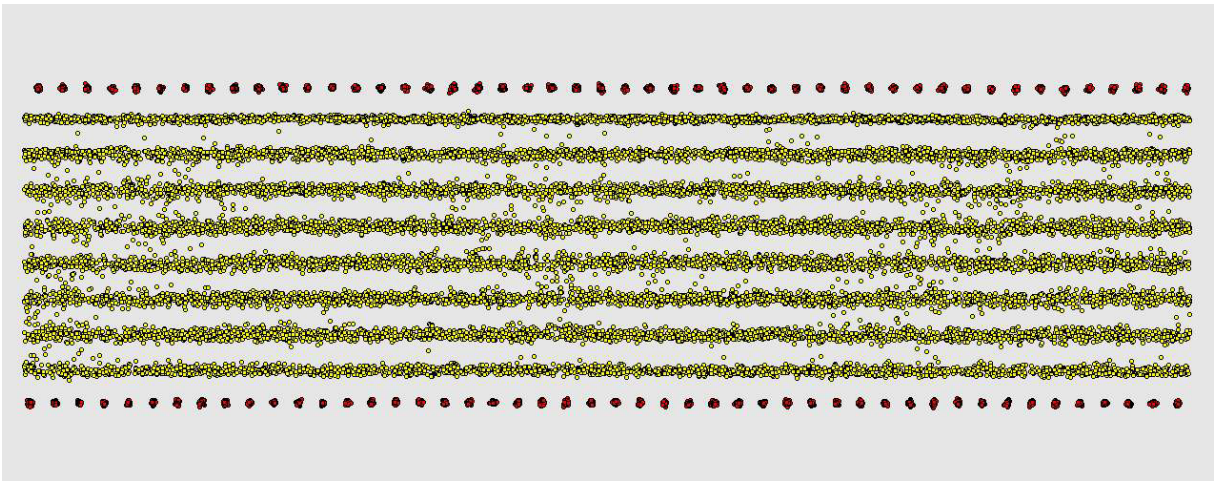

Fig. 8. Side view (xz-plane) of the contact between an elastic block with a flat surface and a flat elastic substrate (only the interfacial layers of atoms are shown) including 1000 $C_{20}H_{42}$ lubricant molecules. Applied pressure $p = 10\,\text{MPa}$; temperature $T = 300\,\text{K}$. The block is moving to the right with velocity $v = 10\,\text{m/s}$. The metal-polymer system is presented after sliding the distance 1400 Å. Eight distinct monolayers of molecules are clearly seen.

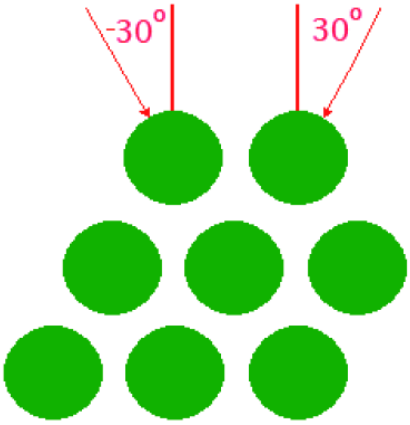

Fig. 9. A schematic view of the 3D domains observed in the lower snapshot of Figure 7. 3D domain represents a 3D region with the close-packed hexagonal structure of almost parallel $C_{20}H_{42}$ molecules.

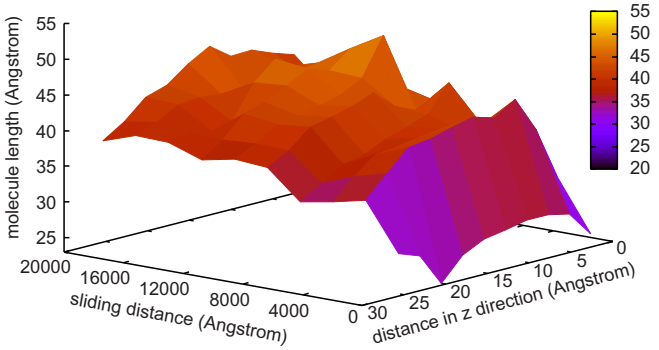

Fig. 10. The average length in the x-direction of the molecules for $C_{100}H_{202}$ polymer-polymer during run-in, as a function of the z-position and the sliding distance, for the sliding velocity $v = 100\,\mathrm{m/s}$ and the applied pressure $p = 10\,\mathrm{MPa}$. The molecules in the center of the contact align faster than those adsorbed to the surfaces.

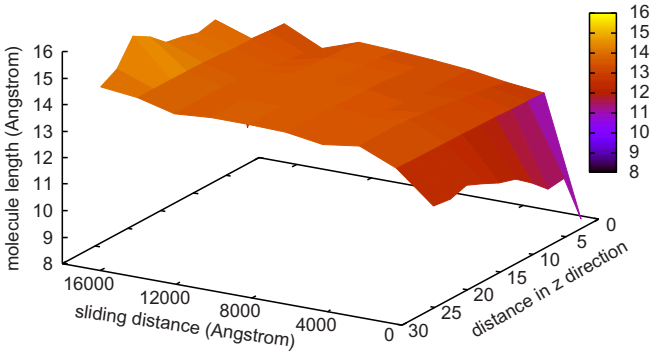

Fig. 11. The average length in the x-direction of the molecules for $C_{20}H_{42}$ polymer-polymer sliding during run-in at velocity of the block $v = 10\,\mathrm{m/s}$ for the applied pressure $p = 10\,\mathrm{MPa}$ as a function of the z-position and the sliding distance. Note that the immobile molecules close to the substrate do not reach the same alignment in the x-direction as do the remaining molecules.

if the wall-film interaction is stronger [7]. So the domains move with the average velocity $v_x \approx 10\,\mathrm{m/s}$. This is because the whole polymer is attached to the block and moves (in average) with the block velocity.

In Figure 9 we present a schematic view of the 3D domain observed in Figure 7 (lower snapshot). In the figure $C_{20}H_{42}$ molecules which form one 3D domain are aligned parallel to each other and are stretching in the x-direction (x-axis directed from us, y-axis directed to the left, z-axis directed up). The figure represents the yz-plane. It could be assumed that under rather high normal pressure the system (in certain regions) prefers to be close-packed. This is achieved when packing of parallel molecules is hexagonal because this is the most close packing possible for parallel long linear objects like $C_{20}H_{42}$ linear polymer molecules. If now we rotate the system 30° from the normal (yz rotation) and look at it from above in the direction marked "30°" in the figure, we will see the 3D domain as it is observed in Figure 7 (lower snapshot). In this direction we see the molecules one under the other as the ordered regions in Figure 7. We also see the same ordered structure of molecules (one under the other) in 3D domains when we look in the direction marked "−30°" in the figure. So we conclude that 3D domains (with $C_{20}H_{42}$ molecules almost parallel in the x-direction) are the ordered regions with the close-packed hexagonal structure.

The 3D crystalline domains can occupy the whole width of the polymer film from the block to the substrate (8 monolayers observed in Fig. 8) in the case of $C_{20}H_{42}$ polymer sliding on metal. The 3D crystalline domains are also found in the $C_{20}H_{42}$ film in the case of polymer sliding on polymer, but in the latter case the domains only extend a few monolayers in the z-direction.

In Figure 10 we show the average length in the sliding x-direction of the $C_{100}H_{202}$ molecules during run-in, as a function of the z-position and the sliding distance. The result is for polymer sliding on polymer at the velocity $v = 100\,\mathrm{m/s}$ and the applied pressure $p = 10\,\mathrm{MPa}$. The molecules in the center of the contact align faster than those adsorbed to the surfaces. In Figure 11 we show similar results for $C_{20}H_{42}$ during run-in at velocity of the block $v = 10\,\mathrm{m/s}$. Note that in this case very little shear alignment occurs, which is consistent with the result in Figure 6. Note also that the immobile molecules close to the substrate do not reach the same alignment in the x-direction as do the remaining molecules.

4 Dependence of the frictional shear stress σ_f on the pressure p_0

Figure 12 shows the relation, after a 200 nm run-in distance, between the frictional shear stress and the normal pressure for a $C_{100}H_{202}$ polymer slab, when the polymer-metal bond is so strong that no slip occurs at the polymer-metal interfaces. The solid line is a linear fit to the data $\sigma_f = \sigma_c + \beta p_0$, with $\sigma_c = 31.5\,\mathrm{MPa}$ and $\beta = 0.07$. We have also performed calculations for the sliding velocity $v = 1\,\mathrm{m/s}$ but the results are nearly the same as for $v = 10\,\mathrm{m/s}$.

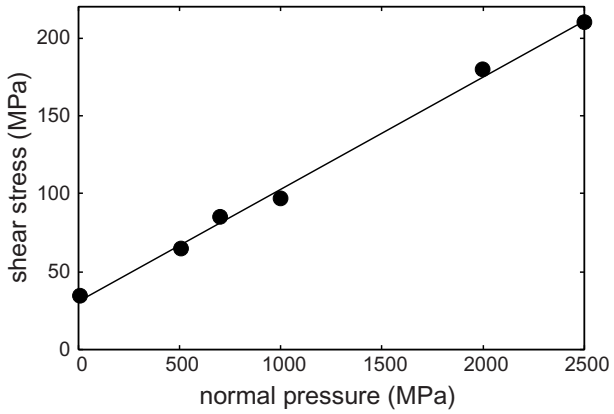

Fig. 12. The relation, after 200 nm run-in distance, between the frictional shear stress and the normal pressure for $C_{100}H_{202}$ polymer slab sliding on $C_{100}H_{202}$ polymer slab (see Fig. 3). Sliding velocity $v = 10\,\mathrm{m/s}$ and background temperature $T = 300\,\mathrm{K}$. The solid line is a linear fit to the data $\sigma_f = \sigma_c + \beta p$, with $\sigma_c = 31.5\,\mathrm{MPa}$ and $\beta = 0.07$.

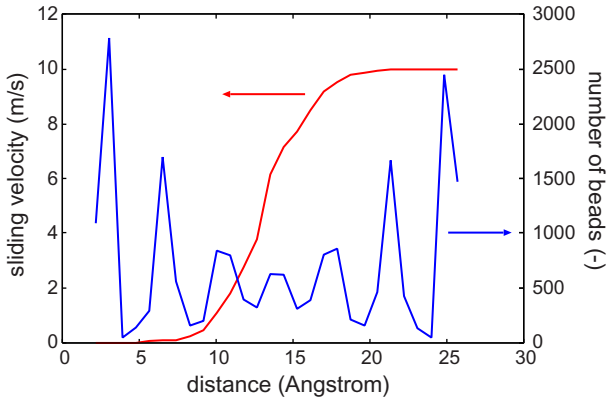

Fig. 13. The velocity profile and the number density of bead units as a function of the distance between the two solid walls, for $C_{100}H_{202}$ polymer slab sliding at the sliding velocity $v = 10\,\mathrm{m/s}$ and background temperature $T = 300\,\mathrm{K}$. Note the strong layering and that most of the slip occurs between the most central layer of lubricant molecules and the two nearby layers.

The value for β found above is very similar to the value found by Rottler and Robbins [22] for the pressure dependence of both the yield stress and the friction of models of glassy polymer where $\beta \approx 0.08$. A similar value (0.07) was found for glassy atomic solids, indicating that sliding at interfaces involving the same glassy solid on both sides of the interface gives a pressure coefficient of the order of ~ 0.06–0.08, independent of the detailed system under study, at least as long as the interaction is of the simple LJ type.

That the slip occurs inside the polymer film, rather than at the polymer-metal interfaces, is illustrated in Figure 13 which shows the velocity profile and the number density of bead units as a function of the distance between the two solid walls. Note the strong layering and that most of the slip occurs between the most central layer of lubricant molecules and the two nearby layers.

When the polymer-metal bond is somewhat weaker than in the study above, slip occurs at the metal-polymer interface. In this case the friction becomes much smaller. This is shown in Figure 14. The solid line is a linear fit to the data $\sigma_f = \sigma_c + \beta p_0$, with $\sigma_c = 1.4\,\mathrm{MPa}$ and $\beta = 9 \times 10^{-4}$. The small magnitude of the friction is related to the fact that the distance between two nearby metal atoms is much smaller than the natural distance between two nearby bead units of two different hydrocarbon molecules; this gives a very weakly corrugated adsorbate-substrate potential energy surface (see below). We note that Bureau *et al.* have observed an order of magnitude change of the shear stress for polymer (PMMA) sliding on strongly and weakly interacting substrates [23].

Note that for very small loads (or squeezing pressures) the frictional shear stress depends non-linearly on the load. A similar non-linear dependence of the nominal shear stress on the load has been observed experimentally by Bureau *et al.* [11] for PMMA in contact with smooth glass surfaces. We have analyzed snapshot pictures which indicate that in the present case the newly prepared polymer

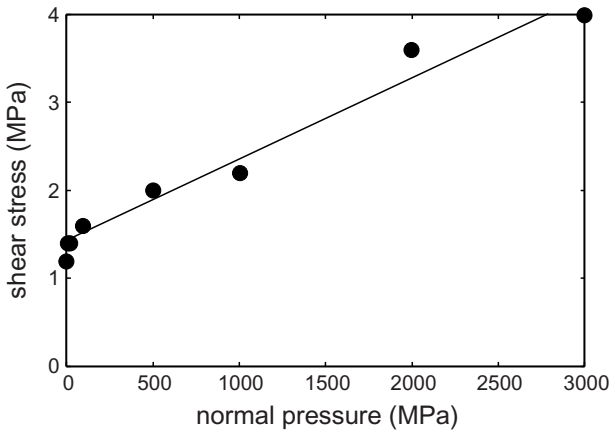

Fig. 14. The relation between the frictional shear stress and the normal pressure for $C_{100}H_{202}$ polymer slab sliding on a "metal" surface (see text for details). Sliding velocity $v = 10\,\mathrm{m/s}$ and background temperature $T = 300\,\mathrm{K}$. The solid line is a linear fit to the data $\sigma_f = \sigma_c + \beta p$, with $\sigma_c = 1.4\,\mathrm{MPa}$ and $\beta = 9 \times 10^{-4}$.

film exhibits surface roughness, which gets smoothened out as the two solids are squeezed together with increasing load. This will increase the contact area and the nominal shear stress will therefore increase in a non-linear way with the load. At least for thick enough polymer films, the surface roughness is likely to be due to frozen capillary waves [24, 25] and the non-linear behaviour may be explained using contact mechanics theory [25].

We have studied the sliding friction for several other polymer systems with chain length ranging from C_{20} to C_{1400}, and obtained very similar results as described above for C_{100}. Thus, in all cases, when the wall-polymer interaction is so strong that no slip occurs at the polymer-metal interface, we observe that the slip is localized in a narrow region in the center of the polymer slab.

The results presented above for polymer sliding on polymer are in good agreement with experimental data. Thus, Whitten *et al.* [8] have studied the shear stress when a spherical glass indenter is sliding on different types of polymers. It is likely that polymer molecules will be transfered to the glass surface so that the sliding interface will be polymer against polymer. The experimental data for the frictional shear stress $\sigma_{\rm f}$ as a function of the normal stress or pressure p_0 was fitted to a linear relation

$$\sigma_{\rm f} = \sigma_c + \beta p_0 \, .$$

For four different polymers (PMMA, PS, PPO and PC) it was found that $\sigma_c = 39$, 25, 20 and 17 MPa (average 25 MPa) while the parameter $\beta = 0.10$, 0.13, 0.05 and 0.06 (average 0.09). For the C_{100} system we find $\sigma_c = 31.5$ MPa and $\beta = 0.07$ which are similar to the experimental results. Note also that the frictional stress σ_c is roughly one tenth of the penetration hardness of the glassy polymers.

For polymer sliding on hard smooth substrates, the frictional shear stress will, of course, depend on the interaction potential and the lattice constant of the substrate. However, since most of hard substrates (*e.g.*, metals or metal oxides) usually have much smaller nearest-neighbor distance between the surface atoms than the natural nearest-neighbor distance between bead units of two (nearby) polymer molecules, the pressure dependence of the shear stress will in general be much weaker (*i.e.*, β much smaller) for the polymer-substrate interface than for the polymer-polymer interface.

The basic physics behind the pressure dependence of the frictional shear stress can be understood based on the picture presented in Figure 15 (see also Ref. [26]). During slip the separation between the atoms or molecules at the sliding interface increases by a small amount Δh. This expansion makes a work against the applied pressure p_0 given by $f\Delta h = p_0 a^2 \Delta h$, where a is the block lattice constant. In addition, the binding energy will decrease in the on-top position because of the reduced number of nearest-neighbor substrate atoms (or molecules). If we denote this energy difference by $\epsilon_0 > 0$, we get the energy difference (per unit block atom or molecule)

$$\Delta E = \epsilon_0 + p_0 a^2 \Delta h.$$

If this increase in energy between on-top and bridge positions is fully lost into heat during the slip downhill from the on-top to the bridge position, then

$$\sigma_{\rm f} a^2 b = \Delta E,$$

where b is the substrate lattice constant, giving

$$\sigma_{\rm f} = \frac{\epsilon_0}{a^2 b} + \frac{\Delta h}{b} p_0 \, ,$$

or

$$\sigma_{\rm f} = \sigma_c + \beta p_0 = \beta (p_{\rm ad} + p_0),$$

with $\sigma_c = \epsilon_0/(a^2 b)$, $p_{\rm ad} = \epsilon_0/(a^2 \Delta h)$ and $\beta = \Delta h/b$. For a bridge and on-top positions as in the figure (assuming $a = 2R$, $b = 2r$)

$$\Delta h = R + r - (R^2 + 2Rr)^{1/2} \, . \qquad (2)$$

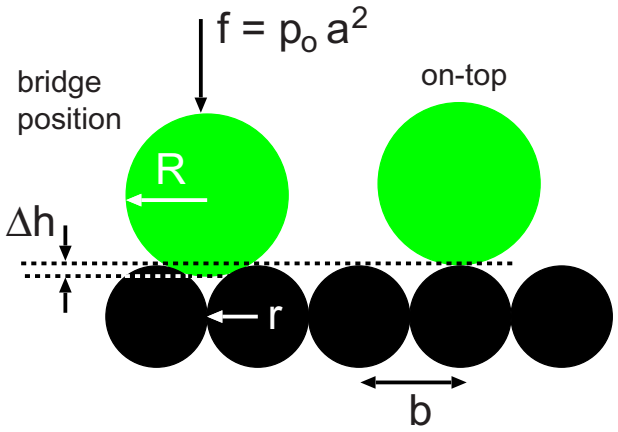

Fig. 15. During slip the separation between the atoms or molecules at the sliding interface increases by a small amount Δh. This expansion makes a work against the applied pressure p_0 given by $U = f\Delta h = p_0 a^2 \Delta h$, where a is the block adsorbate constant. If all the pressure-induced increase in energy is dissipated in the rapid slip downhill from the on-top to bridge position, then $\sigma_{\rm f} a^2 b = U$, where b is the substrate constant.

For the polymer-polymer sliding interface, $r = R$ (and $b = a = 2R$) we get $\Delta h = (2 - \sqrt{3})R$ and $\beta = \Delta h/b = 1 - \sqrt{3}/2 \approx 0.13$, which is similar to the molecular dynamics result for polymer sliding on polymer and experimental results presented above. The estimation of Δh using the geometrical argument presented above is very crude. In the present case an accurate estimate of Δh for the molecule-metal slip interface can be obtained from the potential energy surfaces calculated by adding up the Lennard-Jones interaction potential between a hydrocarbon bead unit and the substrate atoms. For more complex adsorbate-substrate interactions the potential energy surfaces can be deduced (or estimated) using electronic structure calculations. In general Δh rapidly decreases as the ratio R/r increases, *e.g.*, $\Delta h \approx r^2/2R$ (and thus $\beta \approx r/4R$) according to (2) when $R/r \gg 1$. The case $R/r > 1$ will prevail in most cases if the slip occurs not within the polymer film but at one of the metal-polymer interfaces. Indeed in this latter case we observe a much smaller value for β (see Fig. 14) while $p_{\rm ad}$ is similar ($p_{\rm ad} \approx 0.5$ and 1.5 GPa for slip at the polymer-polymer and polymer-metal interface, respectively).

In the analytical calculation presented above we have neglected the influence of temperature (or thermal fluctuations) on the process of "going over the barrier". That is, it was assumed that the external applied tangential force (or stress) alone pulls the system over the lateral pinning barriers, and that this happen everywhere simultaneously. At the high sliding velocities used in our MD simulation, thermal effect should be rather unimportant. However, for small sliding velocities, thermal fluctuations will be very important. In this case slip will not occur everywhere simultaneously, but small nanometer-sized interfacial regions of linear size D will be individually pinned and perform stress-aided thermally induced jump from

one pinned state to another (local interfacial rearrangement processes). (Note that thermal effects can only become important for small (nanometer-sized D) regions, since simultaneous going over the barrier everywhere requires infinitely large energy for an infinite system, except, perhaps for an incommensurate interface.) This process has been studied in detail both theoretically [27–30] and experimentally [31,32].

We emphasize that the effective corrugation of the interaction potential experienced by the molecules at the sliding interface is the most important parameter influencing the magnitude of the friction and the dependence on the external (squeezing) potential. Indeed, the fact that the lattice constant of the substrate is much smaller than the size of the polymer molecules and also very different from the natural separation between the polymer molecules implies that the effective corrugation of the interaction potential between the polymer and the "metal" substrate will be very small, and this explains the small friction observed in this case, compared to the case when the slip occurs at the polymer-polymer interface.

The linear relation between the frictional shear stress and the normal (or squeezing) pressure found above has also been observed in MD calculations for other systems, *e.g.*, in reference [33] for a low concentration of molecules between solid walls with incommensurate atomic structures. In reference [33] it was argued that this is the origin of the proportionality between the friction force and the normal load (the Amontons' law) observed in most practical situations. However, we do not believe that this is the correct explanation in most cases. Rather, almost all surfaces in nature or in engineering applications have surface roughness on many different length scales. In these cases contact mechanics theories predict that the area of real contact is proportional to the load and the stress distribution in the contact region is independent of the load. In this case the Amontons' law will follow, independent of how the frictional shear stress depends on the load. For very smooth surfaces or for elastically soft solids, contact may occur everywhere in the nominal contact area, but in this case one cannot expect the Amontons' law to hold even if the frictional shear stress is proportional to the load, since the area of contact will now depend nonlinearly on the load, *e.g.*, as $F_{\rm N}^{2/3}$ for a spherical surface in contact with a flat, assuming that the Hertz contact theory can be applied to this situation.

5 Summary and conclusions

We have presented results of molecular dynamics calculations of friction performed for a block sliding on a substrate separated by ≈ 3 nm thick polymer film. Two types of systems were considered: a) a polymer film pinned to one of the solid surfaces and sliding at the other solid surface (the "metal"-polymer case). The second case b) was with the polymer layers pinned to both solid surfaces and shearing at the polymer-polymer interface (the polymer-polymer case). We used linear alkane molecules with the number of carbon atoms 20, 60, 100, 140 and 1400.

The run-in distance increases when the length of the alkane molecules increases. During run-in rearrangement in the polymer film takes place and the molecules tend to align along the sliding direction. The run-in distance is especially long for the $C_{1400}H_{2802}$ polymer-polymer interface, and results in a strong decrease in the shear stress.

The frictional shear stress for the polymer-polymer systems is much higher than for the "metal"-polymer systems. This is due to the same size of the atoms or molecules on both sides for the polymer slip plane resulting in strong interlocking (as for a commensurate interface), while the "metal"-polymer interfaces are incommensurate (the lattice constant of the "metal" substrate is different from the distance between the atoms of the lubricant molecules).

The frictional shear stress is (almost) constant when the applied pressure increases from 0 to 10 MPa, while there is a sharp increase when the applied pressure is increased to 500 MPa. We explain this with the use of the adhesion pressure $p_{\rm ad}$. When the applied pressure $p_0 \ll p_{\rm ad}$, the shear stress is (almost) independent of the applied pressure. When $p_0 > p_{\rm ad}$, the shear stress increases linearly with the applied pressure.

A part of the present work was carried out in frames of the ESF program "Nanotribology (NATRIBO)". Two of the authors (I.M.S. and V.N.S.) acknowledge support from IFF, FZ-Jülich, hospitality and help of the staff during their research visits.

References

1. B.N.J. Persson, *Sliding Friction: Physical Principles and Applications*, 2nd edition (Springer, Heidelberg, 2000).
2. D. Dowson, *History of Tribology*, 2nd edition (Professional Engineering Publishing, London and Bury St Edmunds, UK, 1998).
3. Y. Yamaguchi, *Tribology of Plastic Materials: Their Characteristics and Applications to Sliding Components* (Elsevier, Amsterdam, 1990).
4. T. Ruby, T.J. Herslund, I.M. Sivebaek, *New Tribotester for Polymeric Materials*, in *Proceedings of the 12th Nordic Symposium on Tribology: NT2006-13-52, Helsingør, Denmark, June 7-9, 2006*, edited by P. Klit, S. Eskildsen, J. Jakobsen, I.M. Sivebaek (Technical University of Denmark, 2006) ISBN: 87-90416-19-8.
5. B.J. Briscoe, D. Tabor, J. Adhesion **9**, 145 (1978).
6. C.M. Pooley, D. Tabor, Proc. R. Soc. London, Ser. A **329**, 251 (1972).
7. C. Drummond, N. Alcantar, J. Israelachvili, Phys. Rev. E **66**, 011705 (2002).
8. P.G. Whitten, H.R. Brown, Phys. Rev. E **76**, 026101 (2007).
9. N. Maeda, N. Chen, M. Tirrell, J.N. Israelachvili, Science **297**, 379 (2002).
10. R.C. Bowers, J. App. Phys. **42**, 4961 (1971).
11. L. Bureau, T. Baumberger, C. Caroli, Eur. Phys. J. E **19**, 163 (2006).
12. L.C. Towle, J. Appl. Phys. **42**, 2368 (1971).
13. See, *e.g.*, G. He, M.O. Robbins, Phys. Rev. B **64**, 035413 (2001) and references therein.

14. B.N.J. Persson, P. Ballone, J. Chem. Phys. **112**, 9524 (2000).
15. B.N.J. Persson, V.N. Samoilov, S. Zilberman, A. Nitzan, J. Chem. Phys. **117**, 3897 (2002).
16. I.M. Sivebaek, V.N. Samoilov, B.N.J. Persson, J. Chem. Phys. **119**, 2314 (2003).
17. W.L. Jorgensen, J.D. Madura, C.J. Swenson, J. Am. Chem. Soc. **106**, 6638 (1984).
18. D.K. Dysthe, A.H. Fuchs, B. Rousseau, J. Chem. Phys. **112**, 7581 (2000).
19. C. Drummond, J. Israelachvili, Macromolecules **33**, 4910 (2000).
20. P.J. Flory, *Statistical Mechanics of Chain Molecules* (Wiley Interscience, New York, 1969).
21. M.S. Coute, X.Y. Liu, H. Meekes, P. Bennema, J. Appl. Phys. **75**, 627 (1994).
22. J. Rottler, M.O. Robbins, Comput. Phys. Commun. **169**, 177 (2005).
23. L. Bureau, C. Caroli, T. Baumberger, Phys. Rev. Lett. **97**, 225501 (2006).
24. C. Bollinne, S. Cuenot, B. Nysten, A.M. Jonas, Eur. Phys. J. E **12**, 389 (2003).
25. B.N.J. Persson, Surf. Sci. Rep. **61**, 201 (2006).
26. See, *e.g.*, J.N. Israelachvili, in *Fundamentals of Friction: Macroscopic and Microscopic Processes*, *NATO ASI Ser. E: Appl. Sci.*, edited by I.L. Singer, H.M. Pollock, Vol. **220** (Kluwer Academic Publisher, Dordrecht, 1992); B.N.J. Persson, V.N. Samoilov, S. Zilberman, A. Nitzan, J. Chem. Phys. **117**, 3897 (2002).
27. B.N.J. Persson, Phys. Rev. B **51**, 133568 (1995).
28. B.J. Briscoe, in *Fundamentals of Friction: Macroscopic and Microscopic Processes*, *NATO ASI Ser. E: Appl. Sci.*, edited by I.L. Singer, H.M. Pollock, Vol. **220** (Kluwer Academic Publisher, Dordrecht, 1992).
29. A. Schallamach, Wear **6**, 375 (1963).
30. B.N.J. Persson, A.I. Volokitin, Eur. Phys. J. E **21**, 69 (2006).
31. C. Drummond, J. Israelachvili, P. Richetti, Phys. Rev. E **67**, 066110 (2003); C. Drummond, J. Elezgaray, P. Richetti, Europhys. Lett. **58**, 503 (2002).
32. T. Baumberger, C. Caroli, Adv. Phys. **55**, 279 (2006); T. Baumberger, C. Caroli, O. Ronsin, Eur. Phys. J. E **11**, 85 (2003); O. Ronsin, K.L. Coeyrehourcq, Proc. R. Soc. London, Ser. A **457**, 1277 (2001).
33. G. He, M.H. Müser, M.O. Robbins, Science **284**, 1650 (1999).